Journal of Photochemistry and Photobiology A: Chemistry 219 (2011) 167–179

Contents lists available at ScienceDirect

Journal of Photochemistry and Photobiology A: Chemistry

journal homepage: www.elsevier.com/locate/jphotochem

Invited feature article

Experimental demonstration of the electromagnetic mechanism underlying surface enhanced Raman scattering using single nanoparticle spectroscopy

Tamitake Itoh[a,*], Ken-ichi Yoshida[a], Hiroharu Tamaru[b], Vasudevanpillai Biju[a,c], Mitsuru Ishikawa[a]

[a] Nanobioanalysis Group, Health Research Institute, National Institute of Advanced Industrial Science and Technology (AIST), Takamatsu, Kagawa 761-0395, Japan
[b] Photon Science Center, The University of Tokyo, Tokyo 113-8656, Japan
[c] Precursory Research for Embryonic Science and Technology, Japan Science and Technology Agency, Tokyo, Japan

ARTICLE INFO

Article history:
Received 14 November 2010
Received in revised form 1 March 2011
Accepted 3 March 2011
Available online 21 March 2011

Keywords:
SERS
Plasma (plasmon) resonance
Ag nanoaggregate
Twofold electromagnetic enhancement
Single nanoparticle spectroscopy

ABSTRACT

Nanostructures and nanoparticles of Ag and Au offer large enhancements of optical responses such as optical absorption, Rayleigh and Raman scatterings and their nonlinear counterparts to adsorbed molecules. Such enhancements originate from the strong plasma (plasmon) resonance of Ag and Au and have been widely applied for the sensitive detection of various organic and biomolecules under the terminology of surface enhanced spectroscopy, the most common example being surface enhanced Raman scattering (SERS). Although SERS has turned out to be one of the most sensitive analytical techniques, fundamental issues such as lack of conclusive experimental evidence for validating the mechanism underlying SERS and difficulty to establish potential applications of SERS in daily life limit its recognition. Single nanoparticle spectroscopy due to its ability to correlate enhanced Raman scattering with other optical properties of metal nanoparticles is a powerful method for clarifying the mechanism underlying SERS. In this article, we review our recent advances in the experimental evaluation of SERS mechanism. In particular, using single nanoparticle spectroscopy, we attempted to quantitatively evaluate the enhancement mechanism underlying SERS at the onset of electromagnetic (EM) theory. Also, we briefly comment on the advantages of SERS over fluorescence spectroscopy for label-free detection of biomolecules by taking examples from our own investigations and recent reports by others.

1. Introduction

The spectroscopy of enhanced optical responses such as absorption, Rayleigh and Raman scattering and their nonlinear counterparts in the IR to visible region for molecules adsorbed on Ag and Au nanostructures is widely known as surface enhanced spectroscopy, the most common examples being surface enhanced Raman scattering (SERS) and surface enhanced hyper Raman scattering (SEHRS) [1–4]. In particular, huge enhancement factors of SERS (up to 10^{14}) allow us to sensitively measure spectra of analytes at single molecule level [5–9]. SERS spectra are composed of many vibrational bands, which reflect molecular structures and enable us to pinpoint molecular species without the use of conventional fluorescent labels. The high-sensitivity and selectivity of SERS motivated researchers to extend its application towards biotechnology [10–13]. This extension was mostly triggered by the introduction of single-molecule SERS detection [5–9], the developments in nanotechnology that enabled the preparation of sophisticated metal nanostructres [13–15] and the advancements in theoretical calculation including finite-difference time-domain (FDTD) method [7,16–19].

Despite the significant impact of SERS in basic research, fundamental issues such as lack of conclusive experimental evidence for validating the mechanism underlying SERS and difficulty to establish potential applications of SERS in daily life limit its public recognition. We have undertaken different approaches to address the above two issues. We attempted to resolve the first issue by identifying causal relation between the origins of surface enhancement and enhanced optical responses, because these two possible origins were proposed by many researchers [2,3]. Solution to the second issue should come from several trial-and-error attempts in our search for unknown applications of SERS. In this article, we review two mechanisms underlying SERS, which were proposed based on two different origins of surface enhancement. The two mechanisms are called the EM mechanism and the chemical one [2,3]. The EM mechanism is characterized by twofold EM enhancement of Raman scattering signals of molecules adsorbed on metal nanostructures; the first enhancement is due to coupling of plasma resonance with incident light and the second enhancement is due to coupling of plasma resonance with Raman scattering light [2,7,16,17,19–24]. Here we adopt "plasma resonance" in place of the widely used terminology "plasmon resonance" because

* Corresponding author. Tel.: +81 87 869 3557; fax: +81 87 869 4113.
E-mail address: tamitake-itou@aist.go.jp (T. Itoh).

1010-6030/$ – see front matter © 2011 Elsevier B.V. All rights reserved.
doi:10.1016/j.jphotochem.2011.03.001

plasmon means quanta of plasma oscillation inside a metal, which cannot couple with light. Chemical enhancement is characterized by shifting of Raman scattering in non-resonance to that in resonance through the formation of charge transfer complexes between adsorbed molecules and metal surface [3,25–29]. Both mechanisms were experimentally investigated in detail and found to be correct [19,26,27,30–32]. Thus, in an effort to find out which mechanism is dominant, we focused our research on quantitative evaluation of the enhancement factors in different chemical system.

In the present article, we summarize results of our recent experimental investigations to validate the mechanism underlying SERS [19,33–40]. First, using single Ag nanoparticle aggregates, hereafter nanoaggregates, adsorbed with dye molecules, we illustrate quantitative evaluation of the enhancement factors within the framework of EM theory by deducing causal relations among SERS, plasma resonance and shapes of Ag nanoaggregates. In short, single particle spectroscopy enabled us to quantitatively evaluate SERS spectra within the framework of twofold EM enhancement. Finally, we summarize the advantages of SERS over fluorescence spectroscopy for label-free detection of biomolecules by taking examples from our own investigations. Also, we correlate our recent findings with potential applications of SERS [41–43].

2. Evidence of "twofold" EM enhancement

The EM mechanism explains single-molecule SERS sensitivity at interparticle junctions in Ag and Au nanoaggregates based on the fourth power of local EM-field enhancement factors *M*s [7,16,17,19,23,29,43,44]. The twofold EM enhancement factor of SERS $|M|^4$s up to 10^{14} has made sensitive detection of single-molecules realistic [5–9,30,31]. In other words, twofold EM enhancement is important for verifying SERS enhancement factor that enables us to detect single molecules. The first enhancement is due to coupling between incident light and plasma resonance and the second one is due to coupling between SERS light and plasma resonance [2,7,16,17,19–24,33–40]. The relationship among plasma resonance, SERS intensity, and Ag and Au nanoaggregate structures was independently examined to analyze EM enhancement in SERS [30,33–37,45,46]. On the other hand, the first and the second EM enhancements were not independently treated in the previous work, which therefore, failed to provide any conclusive evidence for twofold EM enhancement in SERS.

The twofold EM enhancement provides us with a simple expression for total SERS enhancement by assuming that it is the product of EM enhancement of the incident and scattered light produced by plasma resonance [7,16,17,19,23,30,44,45]. Thus, the total enhancement factor M_{total} of SERS is given by

$$M_{\text{total}} = \left|\frac{E^{\text{Loc}}(\lambda_{\text{L}})}{E^{I}(\lambda_{\text{L}})}\right|^2 \times \left|\frac{E^{\text{Loc}}(\lambda_{\text{L}} \pm \lambda_{\text{R}})}{E^{I}(\lambda_{\text{L}} \pm \lambda_{\text{R}})}\right|^2 = M_1(\lambda_{\text{L}}) \times M_2(\lambda_{\text{L}} \pm \lambda_{\text{R}}) \quad (1)$$

where E^I and E^{Loc} are the amplitudes of the incident and local electric fields, respectively; λ_{L} is the excitation wavelength; $+\lambda_{\text{R}}$ and $-\lambda_{\text{R}}$ are the wavelengths of the anti-Stokes- and Stokes-shifted Raman scattering, respectively; and M_1 and M_2 are the first and the second EM enhancement factors, respectively. The spectrum of $M_2(\lambda)$ is expected to be similar to that of plasma resonance, because the second enhancement was produced by scattering of Raman light through plasma resonance [16,22,23,38–40]. Thus, the dependence of SERS spectra on plasma resonance maxima can be considered to be a key for identifying the second enhancement. However, EM fields on larger Ag nanoaggregates are complex due to overlapping between dipoles and multipoles [47]. Thus, characterization of the dependence of SERS spectra on plasma resonance maxima has been difficult. This difficulty was resolved by selecting Ag nanoaggregates with dipolar plasma resonance that satisfies the following two criteria: polarization dependence of a plasma resonance maximum follows a cosine-squared law, and SERS maxima and plasma resonance maxima have the same polarization dependence to each other. As a consequence of applying these two criteria, we identified coupling of dipolar plasma resonance with SERS [33–37]. The experimental setup for selecting such Ag nanoaggregates is reported elsewhere [48].

We detected Ag nanoaggregate-by-nanoaggregate large variations in the SERS spectra of R6G [5–9]. In the context of second EM enhancement in SERS, the SERS spectral variations of R6G can be explained in terms of the dependence of plasma resonance wavelength on the structure of Ag nanoaggregate because the coupling efficiency between SERS light and plasma resonance depends on the plasma resonance wavelengths. Thus, careful comparison between SERS spectra and plasma resonance spectra would provide convincing evidence for twofold EM enhancement.

Fig. 1A–D shows plasma resonance spectra and SERS spectra of R6G from five Ag nanoaggregates selected from the above two criteria. Note that the SERS bands close to the plasma resonance maxima are selectively enhanced. This selective enhancement shows a correlation between the spectra of SERS enhancement factors and plasma resonance maxima. Thus, the selective enhancement should provide us with a possibility to verify second EM enhancement in SERS. Fig. 1E summarizes the plasma resonance maxima dependence of the anti-Stokes to Stokes intensity ratios for SERS maxima at 553 nm (+634 cm^{-1}) and 580 nm (−634 cm^{-1}). According to Eq. (1) this ratio is given by $M_1(\lambda_{\text{L}})M_2(\lambda_{\text{L}} - \lambda_{\text{R}})/M_1(\lambda_{\text{L}})M_2(\lambda_{\text{L}} + \lambda_{\text{R}})$. Thus, the first EM enhancement factor $M_1(\lambda_{\text{L}})$ cancels. This reduction in the ratio, $M_2(\lambda_{\text{L}} - \lambda_{\text{R}})/M_2(\lambda_{\text{L}} + \lambda_{\text{R}})$, can be correlated with a decrease in the coupling efficiency of anti-Stokes light and plasma resonance due to separation of the plasma resonance maxima from anti-Stokes bands. This correlation supports the conjecture that the second EM enhancement is associated with the origin of variations in anti-Stokes and Stokes SERS spectra.

Fig. 1F–H shows excitation wavelength dependence of SERS spectra for single Ag nanoaggregates and the plasma resonance maxima dependence of SERS spectra for R6G. SERS spectra of the aggregate excited at 568 and 647 nm are shown in Fig. 1G and H, respectively. The intensities of SERS bands around 630 nm in Fig. 1G, and 660 nm in Fig. 1H are larger than those around 588 nm and 710 nm. It is apparent that the SERS bands close to the plasma resonance maxima are selectively enhanced and that this effect is excitation wavelength dependent. These observations demonstrate that second EM enhancement is involved in the enhancement of SERS intensity.

By the correlation between SERS spectra and plasma resonance spectra we could establish that variations of SERS spectra originate from selective enhancement of SERS bands for which the spectral maxima are close to the plasma resonance maxima. In other words, the origin of the variations in the second EM enhancement is due to coupling of SERS light with plasma resonance. However, this consideration does not completely exclude the uncertainty due to inhomogeneity in the measurements of many nanoaggregates. To exclude such an uncertainty, the optical property that plasma resonance maximum sensitively depends on the refractive index of the surrounding media [49–51] was applied to the demonstration of the EM mechanism. From the above relation between SERS and plasma resonance spectra we expect that twofold EM enhancement factors depend on the refractive index, which implies that SERS spectra can be changed by increasing the refractive index of the surrounding medium. The experimental confirmation of this logical connection does not need spectral measurements on many Ag nanoaggregates, because plasma resonance of single Ag nanoaggregates can be changed by simply replacing the surrounding medium and checking the expected spectral changes in SERS.

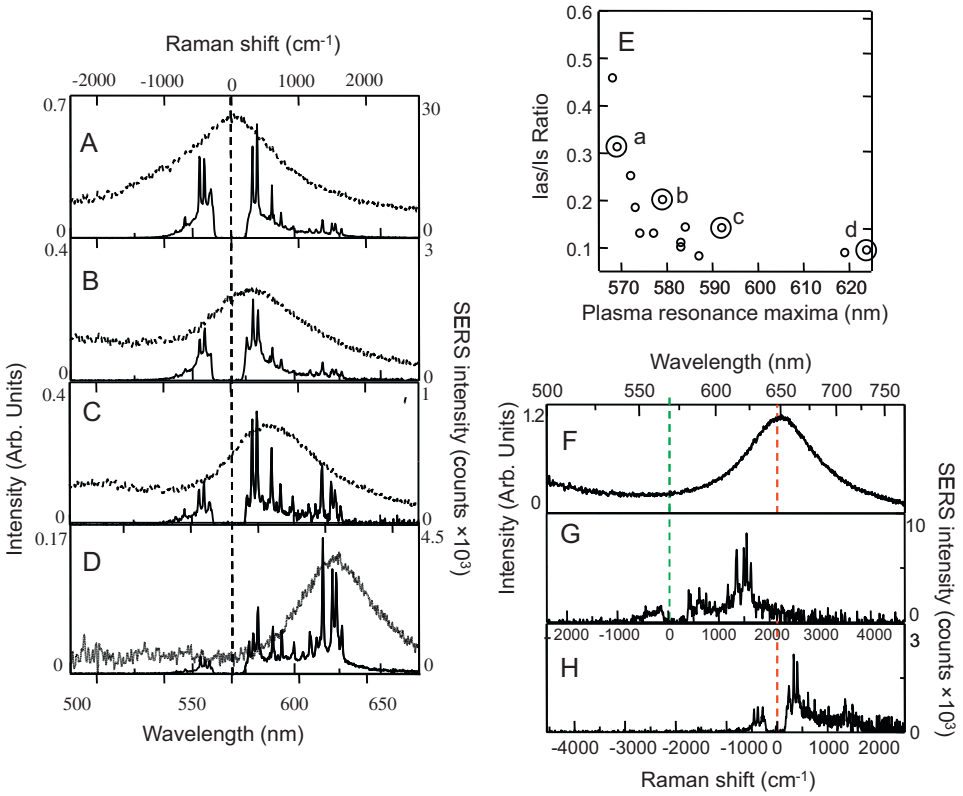

Fig. 1. (A–D) Anti-Stokes and Stokes SERS spectra (solid lines) and plasma resonance spectra (dotted lines) from four representative Ag nanoaggregates. The vertical dashed line indicates the excitation laser wavelength. Plasma resonance maxima in (A–D) were observed at 568, 577, 588, and 623 nm. (E) Plasma resonance maxima dependence of anti-Stokes to Stokes intensity ratios. Doubly circled points indicated by (a–d) correspond to the data in Fig. 1(A–D). (F) Plasma resonance spectra, (G) SERS spectra excited at 568 nm, and (H) SERS spectra excited at 647 nm. All spectra in (F–H) were obtained from the same Ag nanoaggregate.
Taken from Ref. [38].

To investigate dependence of plasma resonance and SERS spectra on the refractive index of the surrounding medium, we measured their spectra from single Ag nanoaggregates without and with covering index matching 20 μm thick oil layer (n = 1.5, Immersion oil TYPE-F, Olympus, Tokyo). Ag nanoaggregates in such samples were located at the interface between air (n = 1.0) and glass (n = 1.5). The effective refractive index n_{eff} of the interface is ∼1.3 [49–51]. Thus, Ag nanoaggregates (∼100 nm) were totally covered with oil for which the refractive index is the same as that of glass. Thus, n_{eff} of the interface is 1.5.

Fig. 2A–F shows plasma resonance and SERS spectra from three representative single Ag nanoaggregates without and with an oil layer. Here we could detect red-shifts in the plasma resonance maxima (Fig. 2A–F). The red-shifts are induced by an increase in the refractive index [49–51]. As shown in Fig. 2A–F, large changes are common to SERS spectra and plasma resonance maxima. Such spectral shifts are commonly observed for almost all single Ag nanoaggregates. This observation indicates that the spectral changes in SERS are caused by red-shifts in plasma resonance maxima. The Ag nanoaggregate whose plasma resonance maximum located around 700 nm in Fig. 2E does not show SERS bands when covered with and oil layer. The disappearance of SERS band may be due to the lack of spectral overlap between SERS and the twofold EM enhancement factor.

The changes in the SERS spectra induced by surrounding media are analyzed based on the twofold EM enhancement as indicated in Eq. (1). SERS spectra are calculated as the products of spectra of M_{total} and Raman scattering derived from ensemble Ag nanoaggregates [39]. We calculated spectra of plasma resonance and M_{total} for a dimer of Ag nanoparticles using n_{eff} = 1.3 and 1.5 by the FDTD method. Fig. 3A and B shows that an increase in n_{eff} causes a red-shift in both spectral maximum of the plasma resonance and M_{total}. Fig. 3C and D shows the calculated SERS spectra using n_{eff} = 1.3 and 1.5, respectively. The calculated changes in SERS spectra are consistent with the experimental ones in Fig. 2A–D. This consistency verifies that the SERS spectral changes in Fig. 2A–D are induced by red-shifts in the spectra of EM enhancement factors, which depend on the refractive index of the surrounding medium of Ag nanoaggregates. Fig. 3E shows the plot of the intensity ratios of anti-Stokes (619 nm) to Stokes SERS (707 nm) bands against plasma resonance maxima λ_p. The inset of Fig. 3E shows the calculated ratios against λ_p based on twofold EM enhancement. The calculated ratios using n_{eff} = 1.3 and 1.5 are well consistent with experimental ones.

In this section, Ag nanoaggregate-by-nanoaggregate variations in SERS spectra and refractive index dependence of SERS spectra were examined by comparing SERS spectra with plasma resonance spectra from single Ag nanoaggregates [38,39]. These two results could be well explained by the selective enhancement of SERS bands whose maxima are close to the plasma resonance maxima. The selective enhancement is an evidence for the second enhancement in the EM mechanism of SERS [38,39].

3. Evaluation of twofold EM enhancement factors

Existence of second EM enhancement motivated us to move into detailed investigation of the EM mechanism of SERS [38,39]. Single-molecule sensitivity of SERS has been demonstrated by many researchers using fluorescent molecules including R6G due to their intrinsic large Raman cross-section and strong optical resonance. Thus, we also examined the EM mechanism using R6G. The EM mechanism predicts that in the case of fluorescent molecules, total intensity is composed of enhanced Raman scattering and enhanced

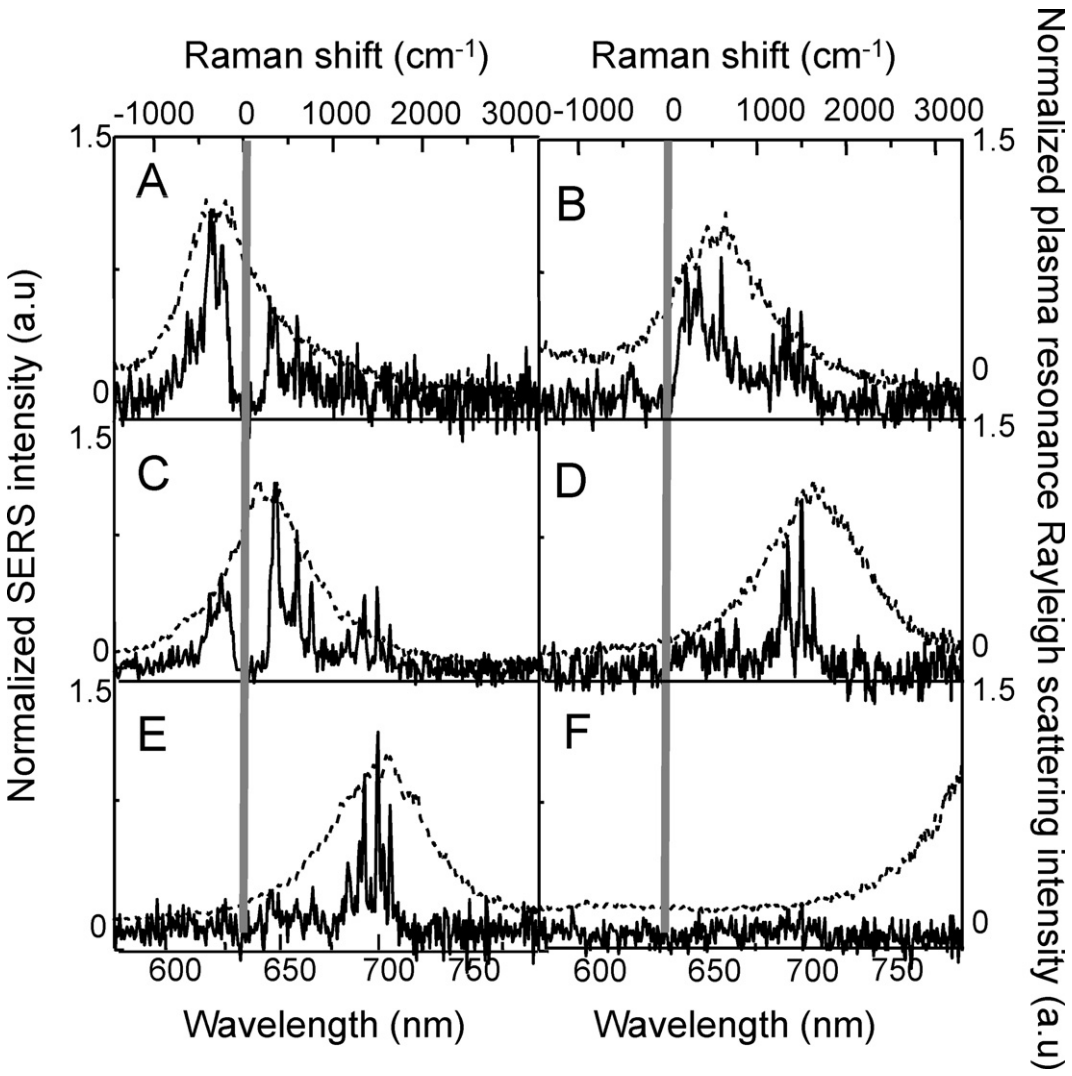

Fig. 2. Plasma resonance and SERS spectra of three representative single Ag nanoaggregates without (A, C, E) and with (B, D, F) covering oil. Taken from Ref. [39].

fluorescence by the following three parameters: a twofold EM enhancement factor induced by plasma resonance $M_1(\lambda_L)M_2(\lambda)$, Raman scattering cross section $\sigma_{RS}(\lambda_L,\lambda)$, and fluorescence cross section $\sigma_{FL}(\lambda_L,\lambda)$ with quenching factors q, excitation wavelength λ_L and Raman scattering wavelength λ [22,23,40,52,53]. The EM mechanism can be quantitatively examined by independently changing three fundamental parameters: $M_1(\lambda_L)M_2(\lambda)$, $\sigma_{RS}(\lambda_L,\lambda)$ plus $q\sigma_{FL}(\lambda_L,\lambda)$, and λ_L. Furthermore, the calculated $M_1(\lambda_L)M_2(\lambda)$ and q also can be correlated with those in the previous reports [22,23,40,52,53].

However, $\sigma_{RS}(\lambda_L,\lambda)$ cannot directly be obtained by experiment because strong fluorescence disturbs us to observe $\sigma_{RS}(\lambda_L,\lambda)$ for fluorescent dye molecules; also $q\sigma_{FL}(\lambda_L,\lambda)$ on a single Ag nanoaggregate without EM enhancement cannot directly be observed [52]. The Stokes Raman spectrum of R6G was observed only after removing strong fluorescence using an ultra fast Kerr shutter [39]. However, low resolution and only the Stokes Raman spectrum do not meet the current requirement for examination. To resolve the issue of the low resolution and the limited spectral region, we obtained $\sigma_{RS}(\lambda_L,\lambda)$ from the high-resolution Stokes SERS spectrum of an ensemble of Ag nanoaggregates. We have already found that spectral shape of plasma resonance of the ensemble Ag nanoaggregates become flat due to the sum of many plasma resonance spectra whose spectral maxima are different from Ag aggregates and randomly distribute in the Stokes region [38,39]. Thus, the spectral shapes of $M_1(\lambda_L)M_2(\lambda)$ of ensemble Ag nanoaggregates are also flat. For this reason, each spectral line within a Stokes SERS of an ensemble Ag nanoaggregate will be uniformly enhanced and the shape of the SERS spectrum becomes equivalent to that of a Raman spectrum. Indeed, we found that the Stokes SERS spectrum of an ensemble Ag nanoaggregate is equivalent to a Raman spectrum [39]. Thus, we used Stokes SERS spectra of ensemble Ag nanoaggregates of each dye as a Stokes Raman spectrum. An anti-Stokes Raman spectrum was calculated using the Stokes SERS spectrum by taking Boltzmann distribution and an effect of resonance enhancement into account [39]. Thus, we obtained the total parameter $\sigma_{RS}(\lambda_L,\lambda)$ by combining the experimental Stokes and the calculated anti-Stokes spectra. Note that the unit of $\sigma_{RS}(\lambda_L,\lambda)$ (photoncount) is converted into cross-section (cm^2) using a calculated Raman profile $\sigma_R(\lambda_L,\lambda)$ of rhodamine molecule [52]. The Raman profile shows excitation-wavelength dependence of Raman spectra. A fluorescence spectrum of each rhodamine molecule in an aqueous solution was substituted for the parameter $\sigma_{FL}(\lambda_L,\lambda)$ because the electronic state of rhodamine molecules physically adsorbed on an Ag surface is equivalent to that in solution [39]. The unit of $\sigma_{FL}(\lambda_L,\lambda)$ (photoncounts) is converted into cross-section (cm^2) using an absorption spectrum derived from Lambert–Beer's law and fluorescence quantum

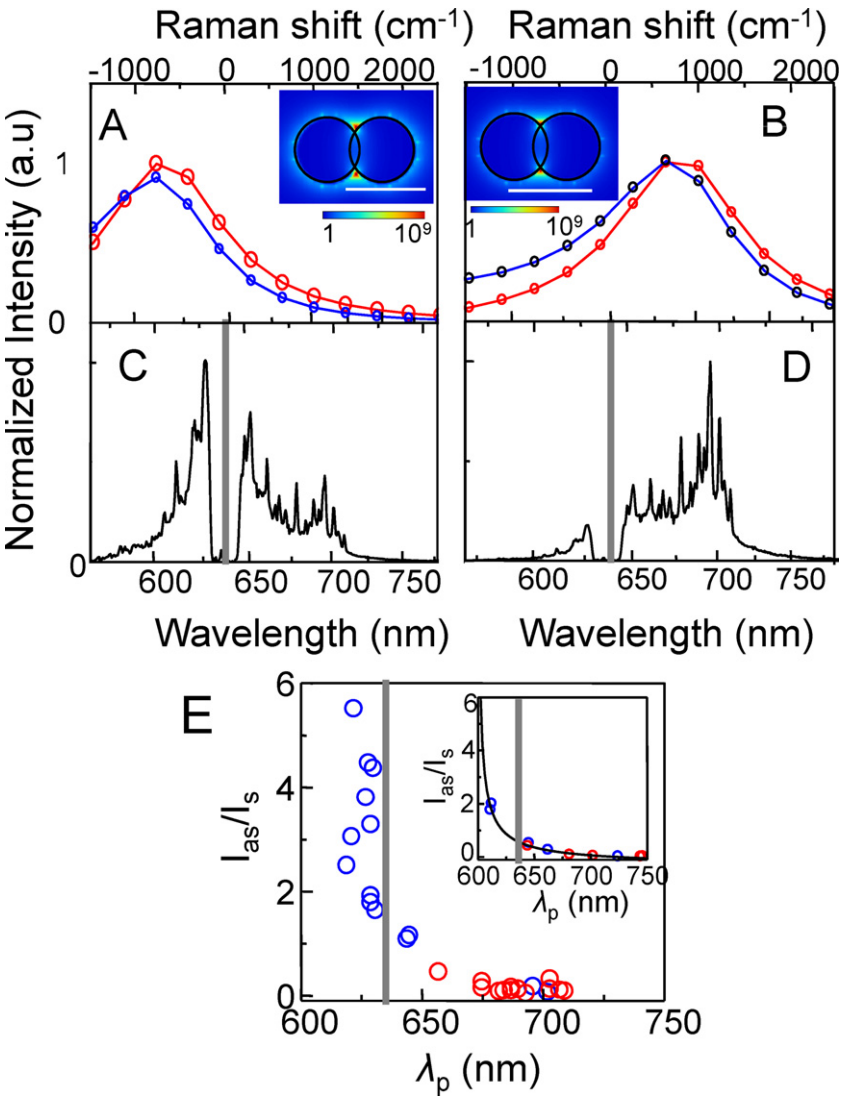

Fig. 3. Calculated spectra of plasma resonance (red lines) and SERS enhancement factors (blue lines) at (A) n_{eff} = 1.3 and (B) n_{eff} = 1.5. Insets: spatial distribution of SERS enhancement factors at plasma resonance maxima. Scale bars are 50 nm. Calculations of SERS spectra at (C) n_{eff} = 1.3 and (D) n_{eff} = 1.5 following Eq. (1). (E) Experiments of λ_p dependence of intensity ratios of anti-Stokes to Stokes SERS bands at 619 nm and 707 nm. Insets: calculations following Eq. (1). Blue and red circles show the ratios of anti-Stokes to Stokes SERS bands at 619 nm and 707 nm without and with covering oil, respectively. (For interpretation of the references to color in this figure legend, the reader is referred to the web version of the article.)
Taken from Ref. [39].

efficiency of R123, R6G, and RB (0.9, 0.95, and 0.70, respectively).

The total emission cross-section spectrum $\sigma_{total}(\lambda_L,\lambda)$ is written as the sum of an enhanced Raman scattering cross-section spectrum $\sigma_{ERS}(\lambda_L,\lambda)$ and an enhanced fluorescence cross-section spectrum $\sigma_{EFL}(\lambda_L,\lambda)$ because both cross section spectra are simultaneously enhanced by plasma resonance within the framework of the EM mechanism [23,40,52]. Thus,

$$\sigma_{total}(\lambda_L,\lambda) = \sigma_{ERS}(\lambda_L,\lambda) + \sigma_{EFL}(\lambda_L,\lambda). \quad (2)$$

A twofold EM enhancement factor spectrum $M_1(\lambda_L)M_2(\lambda)$ as indicated in Eq. (1) is a product of first and second EM enhancement factors. Note that $M_1(\lambda_L)M_2(\lambda)$ is enhancement factor of electric field intensity, not of electric field amplitude. Thus,

$$\sigma_{ERS}(\lambda_L,\lambda) = M_1(\lambda_L)M_2(\lambda)\sigma_{RS}(\lambda_L,\lambda), \quad (3)$$

The parameter σ_{EFL} (λ_L,λ) in Eq. (2) includes the product of EM enhancement of absorption and fluorescence [23,40,52]. The first EM enhancement $M_1(\lambda_L)$ of absorption is equivalent to an increase in the effective absorption cross-section. The plasma resonance coupled with fluorescence light enhances fluorescence by a factor of $M_2(\lambda)$ and simultaneously quenches fluorescence by a factor of q through energy transfer to Ag nanoaggregates [23,40,52]. Thus, quenching factor q is multiplied with $\sigma_{FL}(\lambda_L,\lambda)$ for a molecule free from fluorescence quenching. Thus,

$$\sigma_{EFL}(\lambda_L,\lambda) = M_1(\lambda_L)M_2(\lambda)q\sigma_{FL}(\lambda_L,\lambda). \quad (4)$$

Combination of Eqs. (3) and (4) yields,

$$\sigma_{total}(\lambda_L,\lambda) = M_1(\lambda_L)[\sigma_{RS}(\lambda_L,\lambda) + q\sigma_{FL}(\lambda_L,\lambda)]M_2(\lambda). \quad (5)$$

Now we examine key parameters $M_1(\lambda_L)M_2(\lambda)$, $\sigma_{RRS}(\lambda_L,\lambda)+q\sigma_{FL}(\lambda_L,\lambda)$, and λ_L in Eq. (5). The parameter λ_L was determined by the lasers we used. Thus, we closely examine the ways to evaluate the parameters $M_1(\lambda_L)M_2(\lambda)$ and $\sigma_{RS}(\lambda_L,\lambda)+q\sigma_{FL}(\lambda_L,\lambda)$. The parameter $M_1(\lambda_L)M_2(\lambda)$ can be Lorentzian:

$$M_1(\lambda_L)M_2(\lambda) \propto \frac{1}{(1/\lambda_P - 1/\lambda)^2 + \Gamma^2}, \quad (6)$$

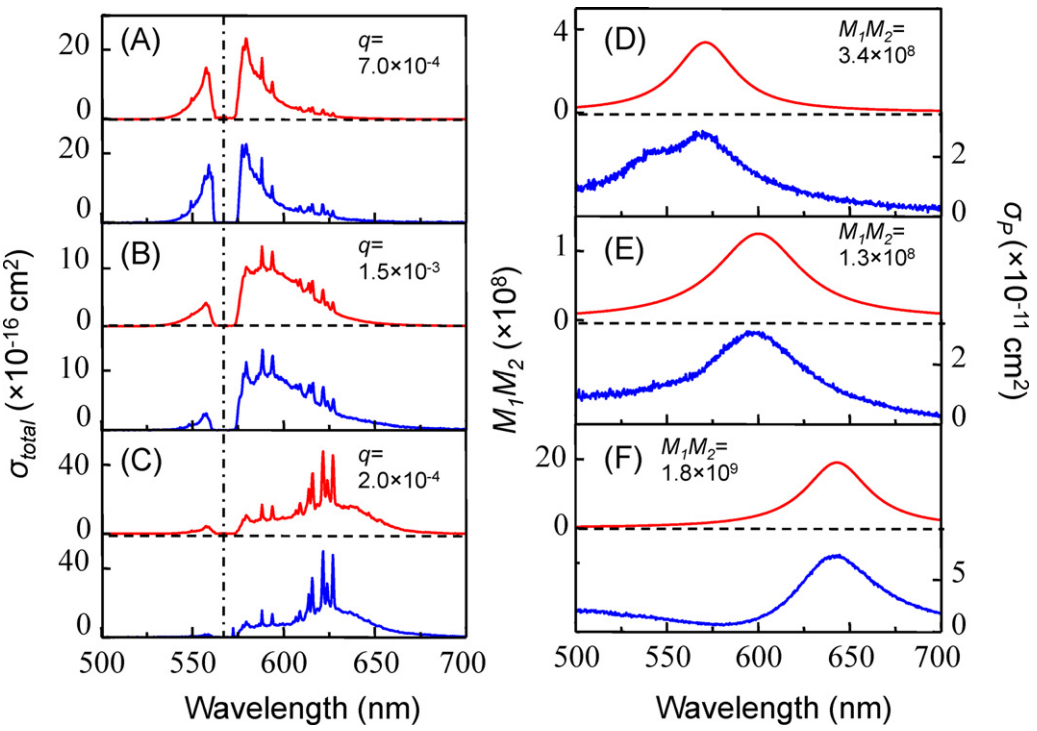

Fig. 4. (A–C) Total emission spectra of R6G calculated by Eq. (5) (red lines) and experimental SERS spectra (blue lines) from three representative nanoaggregates. SERS spectra were excited at 568 nm. (D–F) Spectra of $M_1(\lambda_L)M_2(\lambda)$ (red lines) and experimental plasma resonance spectra (blue lines) from three representative Ag nanoaggregates. Note that left and right axes in (D–F) show $M_1(\lambda_L)M_2(\lambda)$ and the cross-sections of experimental plasma resonance spectra, respectively. The values of q are inserted in (A–C), and the maximum values of $M_1(\lambda_L)M_2(\lambda)$ are inserted in (D)–(F). (For interpretation of the references to color in this figure legend, the reader is referred to the web version of the article.)
Taken from Ref. [40].

where λ_P is the wavelength of plasma resonance; Γ is the linewidth inversely proportional to the dephasing time. Because we selected Ag nanoaggregates showing dipolar plasma resonance, the radiation damping parameter $1/\Gamma$ in this spectral region dominates dephasing of the plasma oscillation. Thus, plasma resonance spectra are close to Lorentzian [54,55]. Here, λ_P and Γ in a Lorentizan line shape in Eq. (6) are assumed to be equivalent to those in an experimental plasma resonance line-shape.

Eq. (5) includes the three parameters; $M_1(\lambda_L)M_2(\lambda)$, $\sigma_{RS}(\lambda_L,\lambda)+q\sigma_{FL}(\lambda_L,\lambda)$ and λ_L. To test Eq. (5) it will be necessary to independently change the three parameters. Thus, we calculated total emission spectra using Eq. (5) and compared those with experimental ones in the following three ways and found consistency between calculations and experiments.

First, $\sigma_{total}(\lambda_L,\lambda)$ from three Ag nanoaggregates with different λ_P and Γ were calculated using Eqs. (5) and (6) for R6G excited at the same λ_L (568 nm). Here, we focus on the parameter $M_1(\lambda_L)M_2(\lambda)$ characterized by experimental λ_P and Γ in Eq. (6). The maximum value of $M_1(\lambda_L)M_2(\lambda)$ and q are fitting parameters. Fig. 4A–C shows three calculated total emission spectra from product of $M_1(\lambda_L)M_2(\lambda)$ and $\sigma_{RRS}(\lambda_L,\lambda)+q\sigma_{FL}(\lambda_L,\lambda)$ (dotted lines) and experimental total emission spectra (solid lines). The calculated total emission spectra well describe characteristics of experimental total emission spectra. Furthermore, Fig. 4D–F show that spectral maxima and line widths similar to those of assumed $M_1(\lambda_L)M_2(\lambda)$ spectra (dotted lines) can be obtained from experimental plasma resonance spectra (solid lines). The similarity shows that plasma resonance dominates $M_1(\lambda_L)M_2(\lambda)$ spectra.

Second, total emission spectra were calculated from three Ag nanoaggregates for R123, R6G and RB excited at λ_L (568 nm). Note that the values of λ_P and Γ for each Ag nanoaggregate are similar to each other. Here, we focus on the parameter $\sigma_{RS}(\lambda_L,\lambda)+q\sigma_{FL}(\lambda_L,\lambda)$ characterized by each dye molecule. In the current calculation, the maximum value of $M_1(\lambda_L)M_2(\lambda)$ and q are fitting parameters. Fig. 5A–C shows calculated total emission spectra (dotted lines) and experimental total emission spectra (solid lines) of R123, R6G, and RB, respectively. The calculated total emission spectra describe the following two characteristics: (i) the enhanced fluorescence intensity from 580 to 650 nm of R123 in Fig. 5A is smaller than that of RB in Fig. 5C, because the fluorescence maximum of R123 (540 nm) is shifted further from plasma resonance maxima (630 nm) than that of RB (580 nm); (ii) the experimental total emission spectra provide characteristics similar to the calculated ones in Fig. 5A–C. This similarity indicates that the total emission spectra can be determined by multiplying $M_1(\lambda_L)M_2(\lambda)$ with $\sigma_{RS}(\lambda_L,\lambda)+q\sigma_{FL}(\lambda_L,\lambda)$.

Third, total emission spectra were calculated using Eq. (5) for R6G at three different λ_Ls. The maximum value of $M_1(\lambda_L)M_2(\lambda)$ and q in $\sigma_{RS}(\lambda_L,\lambda)+q\sigma_{EFL}(\lambda_L,\lambda)$ are fitting parameters. Fig. 6A–C shows calculated total emission spectra (dotted lines) and experimental total emission spectra (solid lines). Both the calculated and experimental total emission spectra show the following two characteristics: (i) overlapping a $M_1(\lambda_L)M_2(\lambda)$ maximum with a Stokes Raman spectrum makes a Stokes SERS dominant in Fig. 6A–B; overlapping of a $M_1(\lambda_L)M_2(\lambda)$ maximum with an anti-Stokes SERS spectrum makes anti-Stokes SERS dominant in Fig. 6C; (ii) the intensity of enhanced fluorescence and SERS spectra in the region of 620–645 nm in Fig. 6A–C is larger than that in the other regions because the $M_1(\lambda_L)M_2(\lambda)$ maximum locates at ~632 nm in Fig. 6D–F. The above two characteristics are exhibited due to a common $M_1(\lambda_L)M_2(\lambda)$ spectral shape in Fig. 6A–C. This means that λ_L dependence of total emission spectral shapes is determined by the product of $M_1(\lambda_L)M_2(\lambda)$ and $\sigma_{RS}(\lambda_L,\lambda)+q\sigma_{FL}(\lambda_L,\lambda)$.

Last, validity of the two fitting parameters is examined. The maximum value of $M_1(\lambda_L)M_2(\lambda)$ in Figs. 4–6 ranges from 6.2×10^7 to 1.9×10^9. The q values in Figs. 4–6 range from 2.4×10^{-5} to 1.5×10^{-3}. Both the estimated values of $M_1(\lambda_L)M_2(\lambda)$ and q in

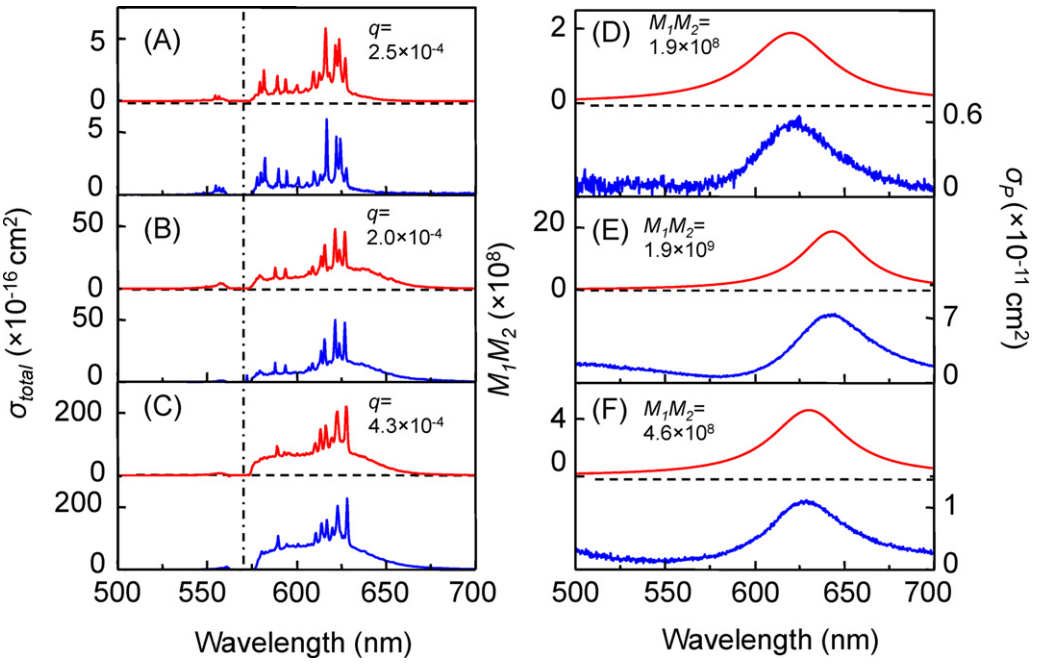

Fig. 5. (A–C) Total emission spectra calculated by Eq. (5) (red lines) and experimental SERS spectra (blue lines, excited at 568 nm in a dashed-and-dotted line) of R123, R6G, and RB, respectively. (D–F) Spectra of $M_1(\lambda_L)M_2(\lambda)$ (red lines) and experimental plasma resonance spectra (blue lines). Note that left and right axes in (D–F) show $M_1(\lambda_L)M_2(\lambda)$ and the cross-sections of experimental plasma resonance spectra, respectively. The values of q are inserted in (A–C), and the maximum values of $M_1(\lambda_L)M_2(\lambda)$ are inserted in (D–F). (For interpretation of the references to color in this figure legend, the reader is referred to the web version of the article.)
Taken from Ref. [40].

the previous work [52] are consistent with those derived from the calculation based on extended Mie theory and Förster-type energy transfer model. The maximum value of $M_1(\lambda_L)M_2(\lambda)$ excited at different λ_L are different from each other. The difference in $M_1(\lambda_L)$ contributed to the difference in the maximum value of $M_1(\lambda_L)M_2(\lambda)$. The maximum value of $M_1(\lambda_L)M_2(\lambda)$ in Fig. 6D–F is 6.2×10^7, 4.4×10^8, and 1.5×10^9, respectively. The ratio of the maximum value of $M_1(\lambda_L)M_2(\lambda)$ in Fig. 6D to that in Fig. 6D–F is 1:7:24. Fig. 6G shows $M_1(\lambda_L)$ factor normalized at 514 nm. $M_1(\lambda_L)$ at 514 nm, 568 nm, and 647 nm are 1, 3, and 24. Thus, the ratio of $M_1(\lambda_L)$ at 514 nm to that at 568 and 647 nm is 1:3:24, both consistent with each other.

In this section the EM mechanism was examined by calculating the total emission spectra by independently changing three essential parameters: twofold EM enhancement factors, Raman plus fluorescence spectra, and excitation wavelengths. Experimental total emission spectra are consistent with the calculated total emission spectra as a function of the three parameters [40]. Furthermore, the calculated twofold EM enhancement factors and fluorescence quenching factors are consistent with those in the previous theoretical work [40].

4. Quantitative evaluation of SERS using morphologies of single Ag nanoaggregates

Quantitative evaluation of the three key parameters of the EM mechanism in the previous section makes us believe that twofold EM enhancement plays a dominant role in SERS [40]. This evaluation provided us with comprehensive guideline to design nanostructures for SERS. However, twofold EM enhancement factors in the previous evaluation were fitting parameters to reproduce experimental spectra [40]. Twofold EM enhancement factors are the functions of plasma resonance, and plasma resonance is a function of the morphology of Ag nanoaggregates. Thus, without measurements of the morphology of Ag nanoaggregates, rigorous calculation of twofold EM enhancement factors is difficult. In this section, plasma resonance and SERS spectra from single isolated Ag nanoaggregates are combined with SEM images to accomplish one-to-one correspondence between optical properties of plasma resonance, that of SERS, and the morphology of Ag nanoaggregates. The experimental observations are compared with FDTD calculations of EM fields based on individual morphology of the Ag nanoaggregates. In this section, we use Raman scattering derived from ensemble Ag nanoaggregates as $\sigma_{RS}(\lambda_L,\lambda) + q\sigma_{FL}(\lambda_L,\lambda)$, not separate $\sigma_{RS}(\lambda_L,\lambda)$ from $q\sigma_{FL}(\lambda_L,\lambda)$ in the evaluation.

Here we add the position coordinate of molecules $\boldsymbol{r}$ in the twofold EM enhancement factor $M_1(\lambda_L)M_2(\lambda)$ to Eq. (1). Thus, $M_1(\lambda_L,\boldsymbol{r})M_2(\lambda,\boldsymbol{r})$ is changed into

$$M_1(\lambda_L,\boldsymbol{r})M_2(\lambda,\boldsymbol{r}) = \left|\frac{E^{loc}(\lambda_L,\boldsymbol{r})}{E^I(\lambda_L)}\right|^2 \times \left|\frac{E^{loc}(\lambda,\boldsymbol{r})}{E^I(\lambda)}\right|^2, \quad (7)$$

where $\boldsymbol{r}$ is an arbitrary position of molecules. To obtain the twofold EM enhancement factor, $M_1(\lambda_L,\boldsymbol{r})M_2(\lambda,\boldsymbol{r})$ in Eq. (7) is summed over the location of dye molecules on the Ag nanoaggregate, and is thus rewritten as

$$\sum_{i=1}^{N} M_1^i(\lambda_L,\boldsymbol{r}_i)M_2^i(\lambda,\boldsymbol{r}_i) \quad (8)$$

M_1^i and M_2^i are the EM enhancement factors of excitation and scattered light at the center of gravity $\boldsymbol{r}_i$ of a molecule i, and N is the total number of molecules. Accordingly, the total cross-section spectra $\sigma_{total}(\lambda_L,\lambda)$ is given by [23]

$$\sigma_{total}(\lambda_L,\lambda) = \sum_{i=1}^{N}[\sigma_{RS}(\lambda_L,\lambda) + q\sigma_{FL}(\lambda_L,\lambda)]M_1^i(\lambda_L,\boldsymbol{r}_i)M_2^i(\lambda,\boldsymbol{r}_i). \quad (9)$$

For an Ag nanoparticle dimer, the largest EM field is generated only at the crevice of Ag nanoaggregates [30], and this largest EM field at the crevice dominates $M_1(\lambda_L,\boldsymbol{r})M_2(\lambda,\boldsymbol{r})$

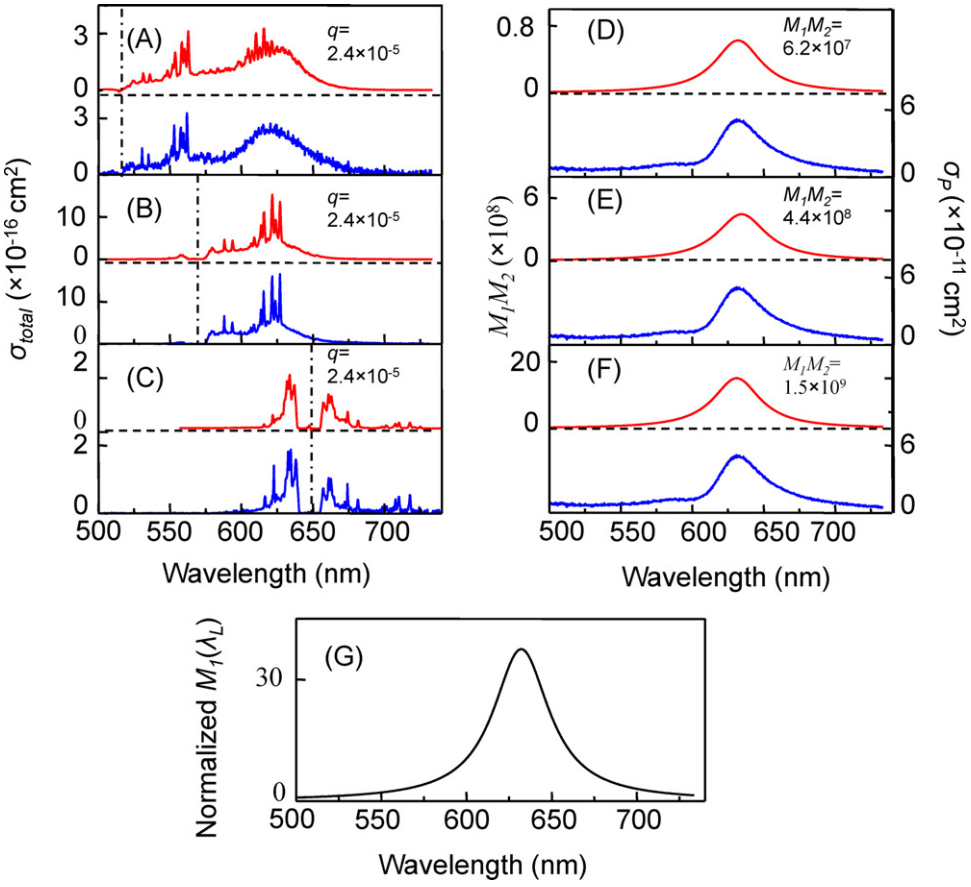

Fig. 6. (A–C) Total emission spectra calculated by Eq. (5) (red lines) and experimental SERS spectra (blue lines, excited at 514, 568, and 647 nm in a dashed-and-dotted lines) of R6G. (D–F) Spectra of $M_1(\lambda_L)M_2(\lambda)$ (red lines) and experimental plasma resonance spectra (blue lines). Note that left and right axes show $M_1(\lambda_L)M_2(\lambda)$ and the cross-sections of experimental plasma resonance spectra, respectively. (G) Wavelength dependence of $M_1(\lambda_L)$. The values of $M_1(\lambda_L)$ are normalized at 514 nm. The values of q are inserted in (A–C), and the maximum values of $M_1(\lambda_L)M_2(\lambda)$ are inserted in (D)–(F). (For interpretation of the references to color in this figure legend, the reader is referred to the web version of the article.)
Taken from Ref. [40].

[23]. Thus, $\sum_{i=1}^{N} M_1^i(\lambda_L, \boldsymbol{r}_i)M_2^i(\lambda, \boldsymbol{r}_i)$ is approximately written as $M_1(\lambda_L,\boldsymbol{r}_o)M_2(\lambda,\boldsymbol{r}_o)$ for a single-molecule in the crevice even if some additional molecules exist at positions other than the crevice. Here, $\boldsymbol{r}_o$ denotes the position at the crevice.

We have identified that most Ag nanoaggregates showing both dipolar plasma resonance and SERS activity are dimers [56]. Theoretical work has predicted that structural anisotropy of Ag dimers induces anisotropy in both plasma resonance and SERS [57,58]. To verify this prediction, we measured anisotropy of both plasma resonance and SERS spectra, and then compared them with FDTD calculations of plasma resonance spectra and $M_1(\lambda_L,\boldsymbol{r})$ using a mesh size 1.5 nm. Fig. 7A–C shows SEM image, the plasma resonance spectra, and the SERS spectra obtained from a Ag dimer. Fig. 7F shows that the FDTD calculations of polarization dependence of a plasma resonance spectrum of the Ag dimer in Fig. 7E could well-reproduce the experimental polarization dependence in Fig. 7B. Fig. 7F and G shows that structural anisotropy of the Ag dimer induces splitting of plasma resonance into the longitudinal mode at 620 nm and transverse mode <400 nm, and coupling of the longitudinal plasma resonance with light polarized along the long axis of the Ag dimer generated the largest $M_1(\lambda_L,\boldsymbol{r})$ at the dimer crevices. The agreement between experimental and calculated polarization dependence suggests that the calculated spatial distribution of $M_1(\lambda_L,\boldsymbol{r})$ in Fig. 7G reflects local EM fields around an Ag dimer. Thus, the SERS in Fig. 7C is generated by EM field coupled with the longitudinal plasma resonance at crevices. Indeed, Fig. 7D and H shows that experimental anisotropy of plasma resonance and $M_1(\lambda_L,\boldsymbol{r})$ well agreed with the calculated anisotropy. Note that $\boldsymbol{r}$ was selected at an arbitrary position in the crevice in Fig. 7I. The agreement is consistent with the prediction by the EM mechanism that anisotropy of Ag nanoaggregates causes anisotropy of SERS.

We must consider the spectral shape of $M_2(\lambda,\boldsymbol{r})$ to evaluate the total spectral shape of $M_1(\lambda_L,\boldsymbol{r})M_2(\lambda,\boldsymbol{r})$ induced by plasma resonance. Fig. 8A–C shows a SEM image of an Ag dimer, an experimental plasma resonance spectrum, and an experimental SERS spectrum, respectively. Fig. 8D–F shows the boundary condition for an Ag dimer in the FDTD calculation, a calculated plasma resonance spectrum, and a spectrum of $M_1(\lambda_L,\boldsymbol{r}_o)M_2(\lambda,\boldsymbol{r}_o)$, respectively. The cross in Fig. 8H indicates the position $\boldsymbol{r}_o$ selected for the calculation of the spectrum in Fig. 8F. Note that we selected $\boldsymbol{r}_o$ at an arbitrary position in the crevice in Fig. 8H simply because we do not consider rigorously the absolute value of $M_1(\lambda_L,\boldsymbol{r}_o)M_2(\lambda,\boldsymbol{r}_o)$ in the calculations in Fig. 8E–G. Fig. 8B and E shows that the experimental plasma resonance spectrum well-agreed with the calculation. The agreement makes confident that the use of the SEM morphology is valid for the boundary condition in the FDTD calculation. Fig. 8E and F shows that the spectral shape of the plasma resonance was quite similar to that of $M_1(\lambda_L,\boldsymbol{r}_o)M_2(\lambda,\boldsymbol{r}_o)$. The similarity is reasonable considering that the EM enhancement is induced by the plasma resonance [23,38–40]. Fig. 8C shows that the SERS spectrum around 610 nm was selectively enhanced by the plasma resonance in Fig. 8B. We found that the selectively enhanced SERS spectra are common to all our experimental results [19,38–40].

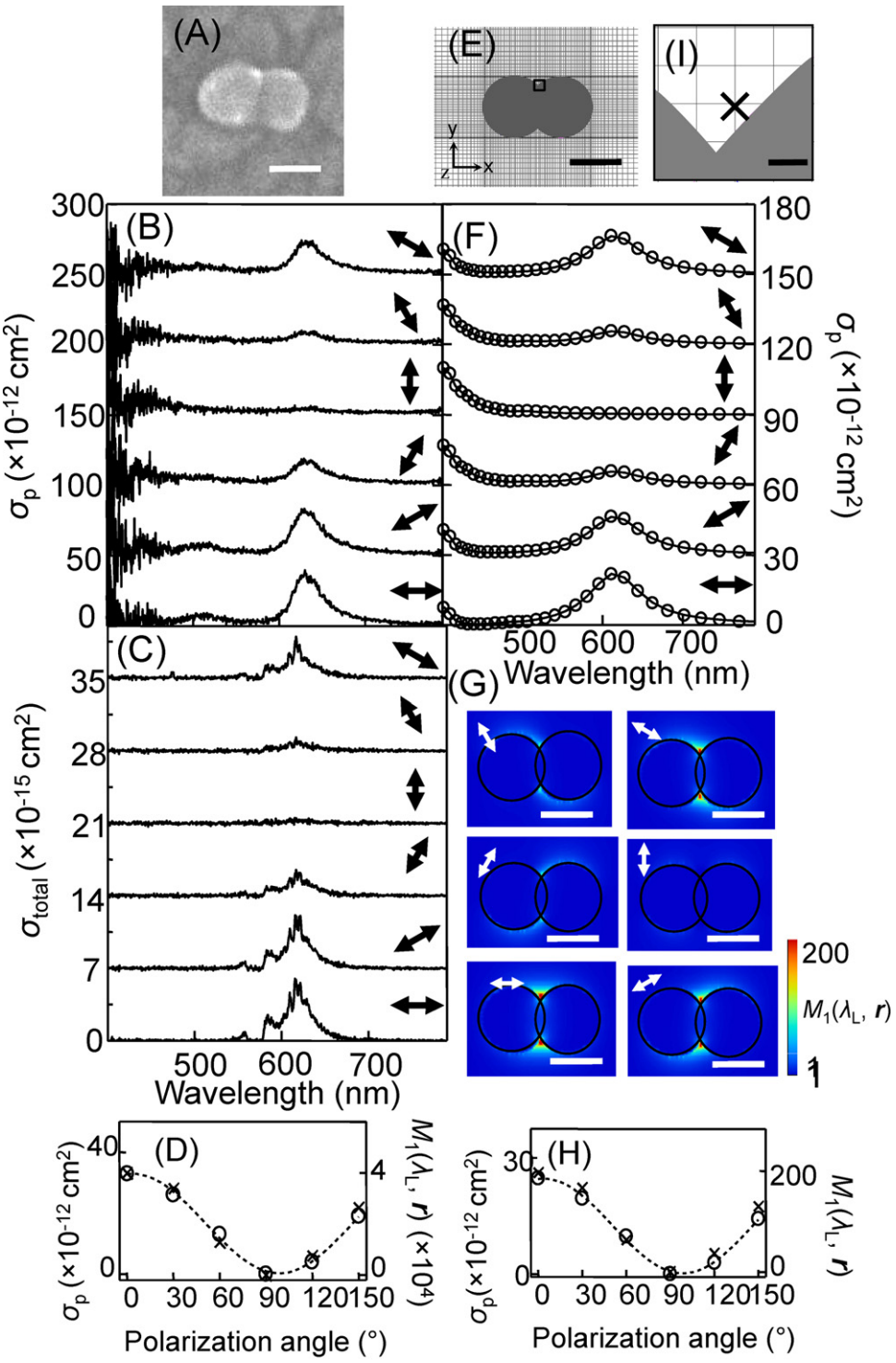

Fig. 7. (A) SEM image, (B) polarization dependence of experimental plasma resonance spectra, and (C) polarization dependence of experimental SERS spectra of a Ag dimer. (D) Polarization angle dependence of cross-sections of experimental plasma resonance (open circles with a dashed curve) and experimental EM enhancement factors (crosses with a dashed curve). (E) Modeled structure of an Ag dimer for the FDTD calculation, (F) polarization dependence of a calculated plasma resonance spectrum, and (G) polarization dependence of calculated spatial distribution of first EM enhancement factors. (H) Polarization angle dependence of cross-sections of calculated plasma resonance (open circles with a dashed curve) and calculated EM factors (crosses with a dashed curve) as a function of polarization angles. (I) Magnified view in the vicinity of the crevice of the Ag dimer in (E). Scale bars in (A, E, G, and I) are 50 nm, 50 nm, 50 nm and 1.5 nm, respectively. Mesh size 1.5 nm, refractive index 1.3 of the surrounding medium, and circularly polarized incident light (532 nm) were selected in the FDTD calculation.
Taken from Ref. [19].

To quantitatively evaluate twofold EM enhancement factors using the FDTD calculation with Yee cells, in which every components of an electric and a magnetic field are set at the center of a side and of a plane in a cubic cell [59], we examined the accuracy in our calculations by comparing FDTD calculations with self-consistent calculation under the common calculation conditions [17]. Note that we did not employ self-consistent calculation because our calculation is limited to asymmetrical Ag nanostructures although self-consistent calculation offers an exact solution to symmetrical Ag nanostructures [17]. We further address an issue

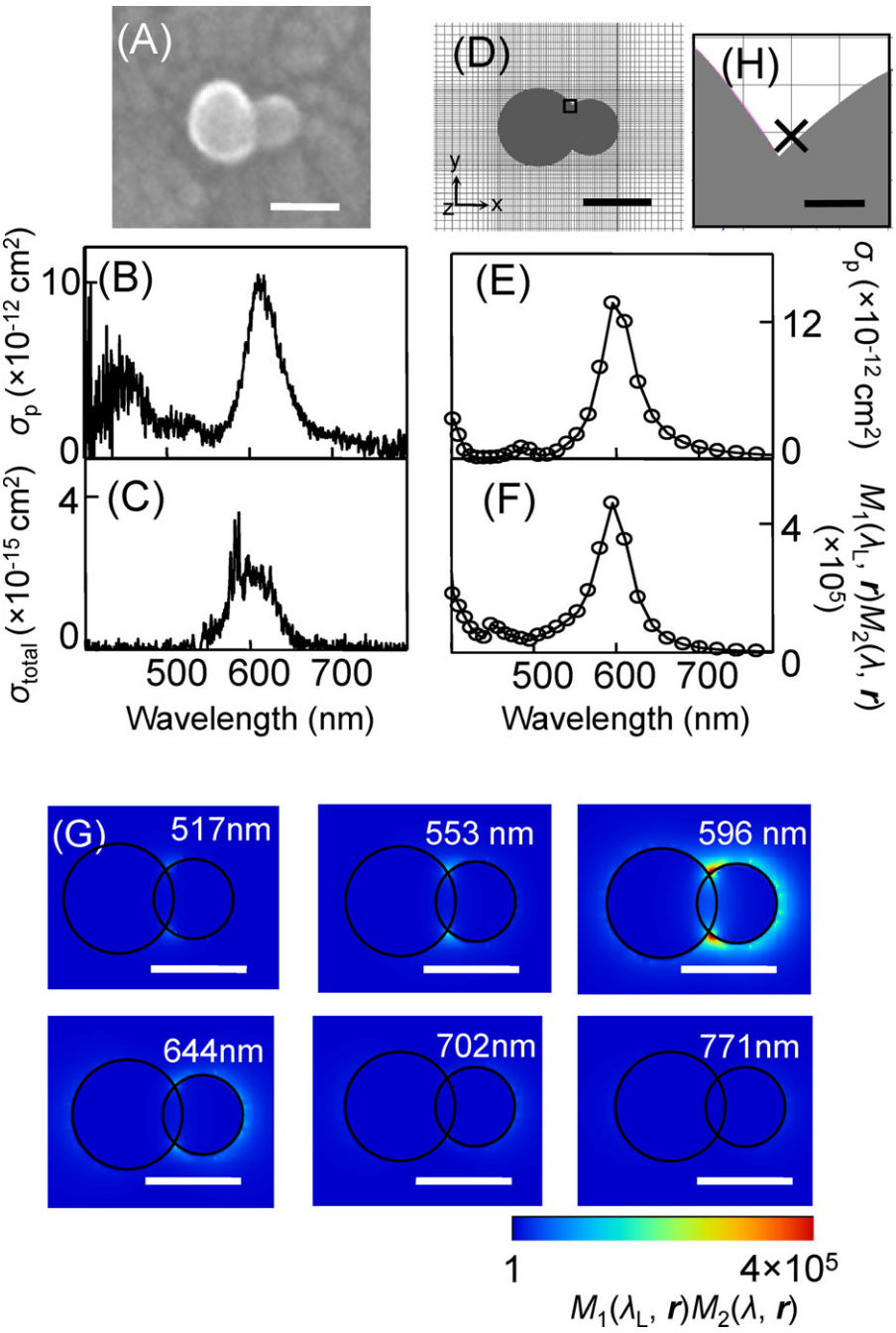

Fig. 8. (A) SEM image, (B) experimental plasma resonance spectrum, and (C) experimental SERS spectrum, (D) modeled structure in the FDTD calculation, (E) calculated plasma resonance spectrum, and (F) calculated spectrum of EM enhancement factor of an Ag dimer. (G) Calculated spectrum of spatial distribution of twofold EM enhancement factors. (H) Magnified view in the vicinity of the crevice of the Ag dimer in (D). The SEM image, the plasma resonance spectrum, and the SERS spectrum in (A)–(C) were observed from the identical Ag nanoparticle. Spectrum of twofold EM enhancement factors in (F) was calculated at the position of cross in (H). Scale bars in (A, D, G, and H) are 50 nm, 50 nm and 1.5 nm, respectively. Mesh size 1.5 nm, refractive index 1.3 of the surrounding medium, and circularly polarized incident light (532 nm) were selected in the FDTD calculation.
Taken from Ref. [19].

about the use of Yee cells in FDTD calculation. The intensity of EM field is maximized at a surface and exponentially decays outside with increasing distance from the surface. However, for a surface having a curvature comparable to mesh size, the calculated exponential decay and the peak intensity of EM field will be smoothed and smaller than the real intensity. This issue leads to underestimation of EM field intensity at the surface, and is not negligible for the surface having small curvature [17]. Fortunately, a factor of underestimation can be reduced by the use of smaller meshes. We selected the morphology of an Ag dimer equivalent to that in Fig. 2A of Ref. [17], and evaluated a factor of underestimation for the dimer with mesh size of 0.98, 0.5, and 0.2 nm; these values are smaller than the gap of the dimer. Fig. 9A shows the morphology of the selected Ag dimer. The *x*-axis is set to overlap with the long axis of the dimer. An EM field reaches the theoretical maximum at the local face-to-face surfaces along the *x*-axis, as shown in the square in Fig. 9A. Note that we used electric flux density instead of an EM field to avoid discontinuity of the field across the surface. Fig. 9B shows the magnified view of the square in Fig. 9A. Fig. 9C shows a spectrum of $M_1(\lambda,\boldsymbol{r})^2$ calculated by the use of mesh size 0.98 nm.

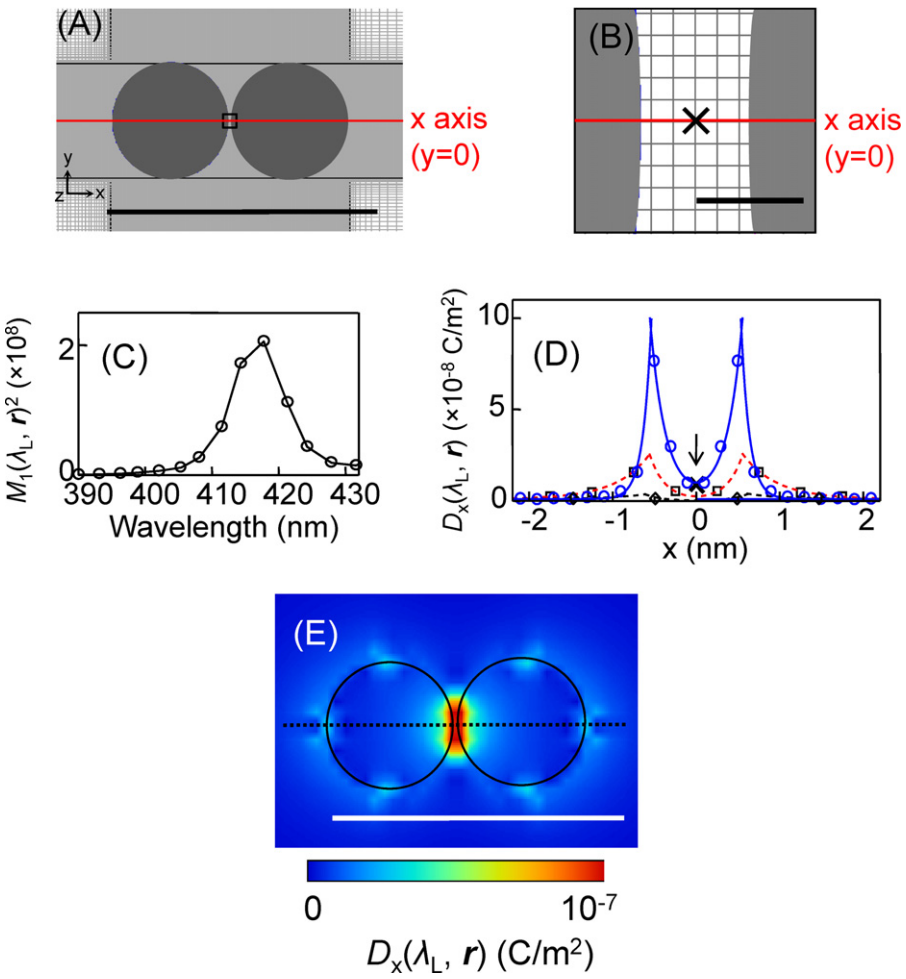

Fig. 9. (A) Modeled structure of an Ag dimer in the FDTD calculation. (B) Magnified view of the vicinity of the gap in the modeled structure. (C) Calculation spectrum of the twofold EM enhancement factor at the cross in (B). (D) Calculated cross-section of spatial distribution of the electric flux density (black broken line, red broken line and blue solid line; mesh size is 1.5 nm, 0.5 nm and 0.2 nm, respectively). (E) Spatial distribution of the electric flux density D_x. The cross-pointed by the arrow in (D) indicates the calculated enhancement factor in Fig. 2(A) of Ref. [17]. Note that the cross-section in (D) indicates the electric flux density along the dashed line in (E). Scale bars in (A, B, and E) is 50 nm, 1.0 nm, and 50 nm, respectively. (For interpretation of the references to color in this figure legend, the reader is referred to the web version of the article.) Taken from Ref. [19].

The spectral maximum locates at ~418 nm, which agrees with Fig. 2A in Ref. [17]. This agreement provides evidence that the plasma resonance for the FDTD calculation of $M_1(\lambda,\boldsymbol{r})^2$ is correct.

Here, we explain the criterion for the accuracy in the calculation of $M_1(\lambda,\boldsymbol{r})^2$. The distance d outside from the surface, where the electric flux density is reduced by a factor of $|1/e|^2$, is defined as $d = \lambda/(2\pi\sqrt{-\varepsilon(\lambda)})$. Here ε is a dielectric constant of Ag (or a vacuum) [60,61]. Along the long axis of a dimer, the ratio of the decay length of bulk Ag d_{Ag} to that of vacuum d_v remains constant ($d_v/d_{Ag} \sim 2.36$) [60,61]. Thus, we can evaluate the accuracy in FDTD calculation from the deviation of the ratio from ~2.36. Fig. 9D shows the decay curves of the electric flux density at 418 nm with several mesh sizes. The ratios evaluated are 0.18, 0.4, and 2.0 with mesh size 0.98, 0.5, and 0.2 nm, respectively. The value of 2.0 is satisfactory considering that FDTD calculation using 0.2 nm mesh requires a computational time longer than 20 days. The calculated electric flux density at the center of the gap is well consistent with self-consistent calculation of Fig. 2B in Ref. [17] as shown by the cross in Fig. 9D.

Finally, we calculate SERS cross-section spectra by the use of mesh size 0.2 nm to quantitatively evaluate twofold enhancement factors. In Fig. 10, we show a set of SERS cross-section spectra acquired from the same dimer with three different incident wavelengths (Fig. 10C–E). The SERS cross-sections were calculated by multiplying $M_1(\lambda_L,\boldsymbol{r}_o)M_2(\lambda,\boldsymbol{r}_o)$ with $\sigma_{RS}(\lambda_L,\lambda)+q\sigma_{FL}(\lambda_L,\lambda)$ using three λ_L (Fig. 10H–J) [40], where $\boldsymbol{r}_o$ (the cross in Fig. 10K) is the location of the center of a R6G molecule. The center locates at ~0.8 nm from the Ag surface. This distance is sufficiently large for blocking charge transfer interaction between R6G molecules and Ag surfaces [62–64]. The shape of the SERS spectra is correctly reproduced in the calculations, and moreover, the experimental cross-sections are consistent with the calculations within a factor of ~2, which is acceptable considering the huge enhancement factor of 10^9 involved in the SERS process. This quantitative consistency of the experimental SERS spectra with the calculations for three incident wavelengths provided us with convincing evidence for the EM mechanism, in which SERS is described as the product of Raman scattering and plasma resonance of the nanostructure [19].

5. Summary and future potential of SERS applications

We have quantitatively investigated the EM mechanism of SERS and demonstrated its absolute validity. Ag nanoaggregate-by-nanoaggregate variations and refractive index dependence of SERS spectra are well-explained by the selective enhancement of SERS bands whose maxima are close to the plasma resonance maxima [38,39]. The selective enhancement is evidence of the second EM enhancement. The EM mechanism was examined by

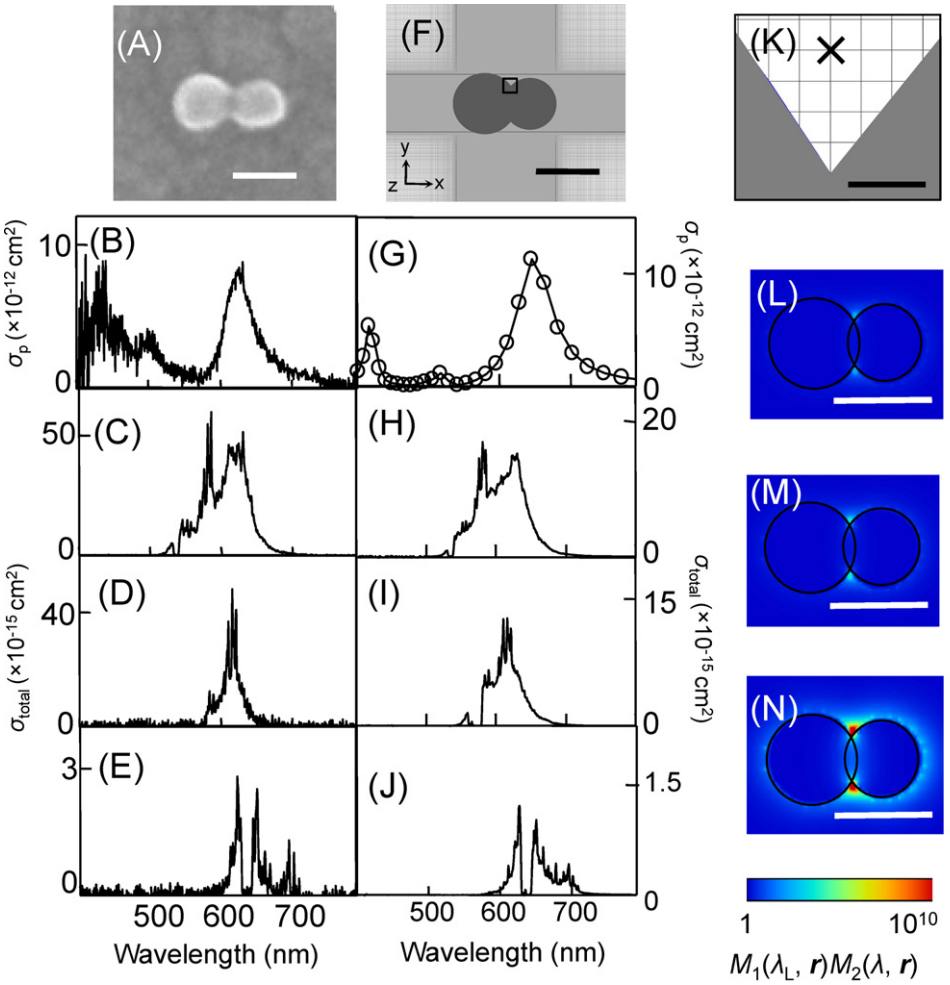

Fig. 10. (A) SEM image of an Ag dimer, (B) experimental plasma resonance spectrum, and experimental SERS spectra excited at (C) 532, (D) 561, and (E) 633 nm. (F) Modeled structure of an Ag dimer in the FDTD calculation, (G) calculated plasma resonance spectrum and calculated SERS spectra excited at (H) 532, (I) 561, and (J) 633 nm. (K) Magnified view in the vicinity of the crevice of the model structure in (F). Spatial distribution of calculated twofold EM enhancement factor excited at (L) 532, (M) 561, and (J) 633 nm. Experimental plasma resonance maximum in (B) was ~620 nm, its FWHM was ~60 nm, and its cross-section was $\sim 1 \times 10^{-11}$ cm^2. Circularly polarized incident light (532, 561, and 633 nm), the mesh size 0.2 nm, and the refractive index 1.3 of the surrounding medium were selected in the FDTD calculation. Scale bars in (A, F, L, and M) are 50 nm. Scale bar in (K) is 0.5 nm.
Taken from Ref. [19].

changing three parameters and calculating SERS spectra: twofold EM enhancement factors, Raman scattering plus fluorescence spectra, and excitation wavelengths. Numerical values of the three parameters with fluorescence quenching factors are consistent with the predicted ones in the frame work of the EM mechanism [23,40]. Experimental observations of plasma resonance, SERS, and morphology of the Ag nanoaggregates were compared with FDTD calculations for the EM field induced by plasma resonance and individual morphology of Ag nanoaggregates [19]. The experimental enhancement factors ~10^9 were consistent with calculations within an error factor of ~2 [19]. We conclusively fortify the indispensible importance of the EM mechanism with our results and extend it to the design of metal nanostructures for generating strong SERS.

In a series of SERS work, Ag/R6G systems were employed as the model system. Here, the chemical enhancement was ignored. However, strong chemical enhancement is reported for Ag/pyridine systems [3,25–29,65]. The chemical enhancement is most likely to depend on the specific target molecules; large molecules such as R6G, for which the resonance is hardly affected by adsorption, is probably reasonable to show diminished chemical enhancement. Our investigations of quantitative nature of the twofold EM enhancement should separate the EM and the chemical enhancement factors and help us to quantify the degree of chemical enhancement in the near future.

Finally let us comment on the application of SERS. Feasibilities of SERS applications have been spread to quite broad fields, from analysis of agrichemicals to label-free ultra-sensitive DNA detections [10–13]. The advantageous points of SERS are high-sensitivity and ability of multiplexed discrimination of several kinds of molecules without the use of fluorescent markers. Fortunately, almost all biomolecules carry amino groups, which have high-affinity for Ag and Au surfaces. Thus, SERS can be an intrinsically potential method for label free detection of biomolecules. We consider that a bottleneck of SERS is the lack of a detailed library of SERS spectra like IR, NMR and Raman scattering spectra. The lack of the library always prevents researchers from practical SERS application. However, the creation of such a library is quite laborious because of SERS spectral fluctuation [5–8,66–69]. Here we report two kinds of our feasibility work for interfacing SERS with biotechnology. First is the detections of biomolecules on the surface of single yeast cells [41,42]. Thanks to the high-sensitivity of SERS, with which we could detect a surface protein in yeast cells at single-molecule level and within 5 s. The detected proteins has tentatively been attributed to a kind of

mannoprotein [41,42]. Second is the detection of low levels of glycated hemoglobin (HbA1c) in the presence of normal hemoglobin (HbA) [44]. Thanks to the detailed spectral structures of SERS, with which we could discriminate HbA1c from HbA molecules within 1 s [43]. Although specific identification of biomolecules by SERS analysis is difficult, development of a detailed library of SERS spectra would be valuable for identifying novel applications of SERS [4,70–76].

Acknowledgements

This work was supported by Scientific Research (19049013) on Priority Area "Strong Photons-Molecules Coupling Fields (470)", Grant-in-Aid for Scientific Research B (20510111), and C (21310071) from The Ministry of Education, Culture, Sports and Science and Technology (MEXT) of Japan, and in part by Precursory Research for Embryonic Science and Technology from Japan Science and Technology Agency and the Photon Frontier Network Program by MEXT.

References

[1] M. Fleischmann, P.J. Hendra, A.J. McQuillan, Chem. Phys. Lett. 26 (1974) 163.
[2] D.L. Jeanmaire, R.P. Van Duyn, J. Electroanal. Chem. 84 (1977) 1.
[3] M. Grant Albrecht, J. Alan Creighton, J. Am. Chem. Soc. 99 (1977) 5215.
[4] D.V. Murphy, K.U. Von Raben, R.K. Chang, P.B. Dorain, Chem. Phys. Lett. 85 (1982) 43.
[5] K. Kneipp, Y. Wang, H. Kneipp, L. Perelman, I. Itzkan, R.R. Dasari, M. Feld, Phys. Rev. Lett. 78 (1997) 1667.
[6] S. Nie, S. Emory, Science 275 (1997) 1102.
[7] H. Xu, E. Bjerneld, M. Käll, L. Borjesson, Phys. Rev. Lett. 83 (1999) 4357.
[8] A. Micheals, M. Nirmal, L. Brus, J. Am. Chem. Soc. 121 (1999) 9932.
[9] J.A. Dieringer, R.B. Lettan II, K.A. Scheidt, R.P. Van Duyne, J. Am. Chem. Soc. 129 (2007) 16249.
[10] Y.C. Cao, R. Jin, C.A. Mirkin, Science 297 (2002) 1536.
[11] X. Qian, X.H. Peng, D.O. Ansari, Q.Y. Goen, G.Z. Chen, D.M. Shin, L. Yang, A.N. Young, M.D. Wang, S.M. Nie, Nat. Biotechnol. 26 (2007) 83.
[12] J.N. Anker, W.P. Hall, O. Lyandres, N.C. Shah, J. Zhao, R.P. Van Duyne, Nat. Mater. 7 (2008) 442.
[13] J.F. Li, Y.F. Huang, Y. Ding, Z.L. Yang, S.B. Li, X.S. Zhou, F.R. Fan, W. Zhang, Z.Y. Zhou, D.Y. Wu, B. Ren, Z.L. Wang, Z.Q. Tian, Nature 464 (2010) 392.
[14] E.M. Hicks, S.L. Zou, G.C. Schatz, K.G. Spears, R.P. Van Duyne, L. Gunnarsson, T. Rindzevicius, B. Kasemo, M. Käll, Nano Lett. 5 (2005) 1065.
[15] K. Ueno, S. Juodkazis, V. Mizeikis, K. Sasaki, H. Misawa, Adv. Mater. 20 (2008) 26.
[16] M. Inoue, K. Ohtaka, J. Phys. Soc. Jpn. 52 (1983) 3853.
[17] H. Xu, J. Aizpurua, M. Käll, P. Apell, Phys. Rev. E 62 (2000) 4318.
[18] H. Kuwata, H. Tamaru, K. Esumi, K. Miyano, Appl. Phys. Lett. 83 (2003) 4625.
[19] K. Yoshida, T. Itoh, H. Tamaru, V. Biju, M. Ishikawa, Y. Ozaki, Phys. Rev. B 81 (2010) 115406.
[20] D. Wang, M. Kerker, Phys. Rev. B 24 (1981) 1777.
[21] M. Moskovits, Rev. Mod. Phys. 57 (1985) 783.
[22] B. Pettinger, J. Chem. Phys. 85 (1986) 7442.
[23] H. Xu, X. Wang, M.P. Persson, H.Q. Xu, M. Käll, P. Johansson, Phys. Rev. Lett. 93 (2004) 243002.
[24] J.R. Lombardi, R.L. Birke, T. Lu, J. Xu, J. Chem. Phys. 84 (1986) 4174.
[25] V. Biju, T. Itoh, A. Anas, S. Sujith, M. Ishikawa, Anal. Bioanal. Chem. 391 (2008) 2469.
[26] A. Otto, I. Mrozek, H. Grabhorn, W. Akemann, J. Phys. Condens. Mater. 4 (1992) 1143.
[27] A. Campion, P. Kambhampati, Chem. Soc. Rev. 27 (1998) 241.
[28] R.L. Birke, V. Znamenskiy, J.R. Lombardi, J. Chem. Phys. 132 (2010) 214707.
[29] D. Wu, J. Li, B. Ren, Z. Tian, Chem. Soc. Rev. 37 (2008) 1025.
[30] K. Imura, H. Okamoto, M. Hossain, M. Kitajima, Nano Lett. 6 (2006) 2173.
[31] E. Le Ru, P. Etchegoin, Chem. Phys. Lett. 423 (2006) 63.
[32] S.A. Meyer, E.C. Le Ru, P.G. Etchegoin, J. Phys. Chem. A 114 (2010) 5515.
[33] T. Itoh, K. Hashimoto, Y. Ozaki, Appl. Phys. Lett. 83 (2003) 2274.
[34] T. Itoh, K. Hashimoto, A. Ikehata, Y. Ozaki, Appl. Phys. Lett. 83 (2003) 5557.
[35] T. Itoh, K. Hashimoto, A. Ikehata, Y. Ozaki, Chem. Phys. Lett. 389 (2004) 225.
[36] T. Itoh, Y. Kikkawa, V. Biju, M. Ishikawa, A. Ikehata, Y. Ozaki, J. Phys. Chem. B 110 (2006) 21536.
[37] T. Itoh, V. Biju, M. Ishikawa, Y. Kikkawa, K. Hashimoto, A. Ikehata, Y. Ozaki, J. Chem. Phys. 124 (2006) 134708.
[38] T. Itoh, K. Yoshida, V. Biju, Y. Kikkawa, M. Ishikawa, Y. Ozaki, Phys. Rev. B 76 (2007) 085405.
[39] K. Yoshida, T. Itoh, V. Biju, M. Ishikawa, Y. Ozaki, Appl. Phys. Lett. 95 (2009) 263104.
[40] K. Yoshida, T. Itoh, V. Biju, M. Ishikawa, Y. Ozaki, Phys. Rev. B 79 (2009) 085419.
[41] A. Sujith, T. Itoh, H. Abe, A.A. Anas, K. Yoshida, V. Biju, M. Ishikawa, Appl. Phys. Lett. 92 (2008) 103901.
[42] A. Sujith, T. Itoh, H. Abe, K. Yoshida, M.S. Kiran, V. Biju, M. Ishikawa, Anal. Bioanal. Chem. 394 (2009) 1803.
[43] M.S. Kiran, T. Itoh, K. Yoshida, N. Kawashima, V. Biju, M. Ishikawa, Anal. Chem. 82 (2010) 1342.
[44] F.J. Garcĭa-Vidal, J.B. Pendry, Phys. Rev. Lett. 77 (1996) 1163.
[45] E. Hao, G.C. Schatz, J. Chem. Phys. 120 (2004) 357.
[46] I. Khan, D. Cunningham, D. Graham, D.W. McComb, W.E. Smith, J. Phys. Chem. B 109 (2005) 3454.
[47] U. Kreibig, M. Vollmer, Optical Properties of Metal Clusters, vol. 25, Springer Series in Materials Science, Springer, Berlin, 1995.
[48] T. Itoh, Y. Kikkawa, K. Yoshida, K. Hashimoto, V. Biju, M. Ishikawa, Y. Ozaki, J. Photochem. Photobio. A 183 (2006) 322.
[49] T. Itoh, T. Asahi, H. Masuhara, Jpn. J. Appl. Phys. 41 (2002) L76.
[50] T. Itoh, T. Uwada, T. Asahi, Y. Ozaki, H. Masuhara, Can. J. Anal. Sci. Spectrosc. 52 (2007) 130.
[51] C. Sönnichsen, S. Geier, N. Hecker, G. Plessen, J. Feldmann, H. Ditlbacher, B. Lamprecht, J. Krenn, F. Aussenegg, V. Chan, J. Spatz, M. Möller, Appl. Phys. Lett. 77 (2000) 2949.
[52] P. Johansson, H. Xu, M. Käll, Phys. Rev. B 72 (2005) 035427.
[53] C.M. Galloway, P.G. Etchegoin, E.C. Le Ru, Phys. Rev. Lett. 103 (2009) 063003.
[54] C. Sönnichsen, T. Franzl, T. Wilk, G. Plsesson, J. Feldmann, O. Wilson, P. Mulvaney, Phys. Rev. Lett. 88 (2002) 077402.
[55] M. Schalaev, E. Poliakov, V. Markel, Phys. Rev. B 53 (1996) 2437.
[56] K. Yoshida, T. Itoh, V. Biju, M. Ishikawa, Y. Ozaki, Proceedings of the XXIth International Conference on Raman Spectroscopy (ICORS), 2008, p. 341.
[57] T. Ambjörnsson, G. Mukhopadhyay, S. Apell, M. Käll, Phys. Rev. B 73 (2006) 085412.
[58] C. Tally, J. Jackson, C. Oubre, N. Grady, C. Hollars, S. Lane, T. Huser, P. Nordlander, N. Halas, Nano Lett. 5 (2005) 1569.
[59] A. Taflove, S. Hagness, Computational Electrodynamics, third edition, Artech House, Norwood, 2005.
[60] T. Ong, V. Celli, A. Marvin, J. Opt. Soc. Am. A 11 (1994) 759.
[61] H. Reather, Surface Plasmons on Smooth and Rough Surfaces and on Gratings, Springer-Verlag, 1988, Chapter 2.
See, for example.
[62] T. Sen, S. Sadhu, A. Patra, Appl. Phys. Lett. 91 (2007) 043104.
[63] T. Sen, A. Patra, J. Phys. Chem. C 112 (2008) 3216.
[64] S. Saini, G. Srinivas, B. Bagchi, J. Phys. Chem. B 113 (2009) 1817.
[65] A. Otto, Phys. Stat. Sol. 188 (2001) 1455.
[66] Y. Maruyama, M. Ishikawa, M. Futamata, J. Phys. Chem. B 108 (2004) 673.
[67] S. Habuchi, M. Cotlet, R. Gronheid, G. Dirix, J. Michiels, J. Vanderleyden, F.D. Schryver, J. Hofkens, J. Am. Chem. Soc. 125 (2003) 8446.
[68] Y. Kitahama, Y. Tanaka, T. Itoh, Y. Ozaki, Phys. Chem. Chem. Phys. 12 (2010) 7457.
[69] Y. Kitahama, A. Ogawa, Y. Tanaka, S. Obeidat, T. Itoh, M. Ishikawa, Y. Ozaki, Chem. Phys. Lett. 493 (2010) 30.
[70] W.H. Yang, J. Hulteen, G.C. Schatz, R.P. Van Duyne, J. Chem. Phys. 104 (1996) 4313.
[71] W.N. Leng, A.A. Yasseri, S. Sharma, Z.Y. Li, H.Y. Woo, D. Vak, G.C. Bazan, A.M. Kelley, Anal. Chem. 78 (2006) 6279.
[72] T. Itoh, Y. Ozaki, H. Yoshikawa, T. Ihama, H. Masuhara, Appl. Phys. Lett. 88 (2006) 084102.
[73] J. Kneipp, H. Kneipp, B. Wittig, K. Kneipp, Nano Lett. 7 (2007) 2819.
[74] K. Ikeda, M. Takase, Y. Sawai, H. Nabika, K. Murakoshi, K. Uosaki, J. Chem. Phys. 127 (2007) 111103.
[75] T. Itoh, H. Yoshikawa, K. Yoshida, V. Biju, M. Ishikawa, J. Chem. Phys. 130 (2009) 214706.
[76] T. Itoh, H. Yoshikawa, K. Yoshida, V. Biju, M. Ishikawa, J. Chem. Phys. 133 (2010) 124704.